DC Solutions of Postbuckling Problems

P. ALART and S. PAGANO
LMGC, Université de Montpellier II – UMR 5508, Place Eugene Bataillon,
34005 Montpellier Cedex, France (*e-mail: alart@lmgc.univ-montp2.fr*)

Abstract. In this paper we present an approach to determine the local minima of a specific class of minimization problems. Attention is focused on the inextensibility condition of flexible rods expressed as a non convex constraint. Two algorithms are derived from a special splitting of the Lagrangian into the difference of two convex functions (DC). They are compared to the classical augmented Lagrangian method used in this context. These DC formulations are easily extended to contact problems and applied to the determination of confined postbuckling shapes and to microbuckling in a cellular structure.

Key words. augmented Lagrangian, confined buckling, difference of convex function (DC), local minimization, non linear mechanics, unilateral contact.

1. Introduction

The study of stability and bifurcation theory for structures is an important topics in mechanics from a theoretical and a practical point of view [14]. Indeed, some instability phenomena can occur for usual thin structures before collapse threshold. Two types of information are required: the critical values of the loading and the postbuckling shapes. As noted by Bloom and Coffin [5], the long history of buckling theory for structures begins with the studies by Euler in 1744 of the stability of flexible compressed beams [10]. It is well known that a force applied to the ends of the rod and oriented according to the rod may lead to different equilibrium states if the magnitude of the force is large enough.

To illustrate this phenomena of bifurcation within the specific context of buckling and postbuckling of structures, we will use the example of the buckling of a thin rod under a compression P. A solution of the classical Euler equation is a quadruple (P, θ, u_1, u_2) where **u** is the displacement field, and any solution with $u_2 \not\equiv 0$ is called a buckled state. The linearized version of this problem, for small displacement **u** and small angles θ, can be written; from this problem we can deduce the critical values and buckling branches around the trivial solution $(P, 0, 0, 0)$. On physical grounds, the picture provided only by the linearized problem is clearly unsatisfactory. Indeed the buckling shapes is known but the size of the deflection u_2 is undetermined. The non linear problem gives a more reasonable prediction of the buckling phenomena since we can reach the

deformed shape. It is very easy to show that the critical values for the non-linear problem are the same than for the linearized one.

In non linear mechanics, and specially when large deformations occur, we have to deal with a non convex potential energy. Consequently, the equilibrium states may be defined as the local minima of this potential. For continuous problems, the local minimum depends on the topology associated with the infinite dimensional spaces of the admissible configurations [16]. The existence and the approximation of local minimizing solutions are still open questions and are out of purpose of this paper. But from a practical point of view, we have to determine numerically local minima in finite dimensional spaces by using the more general way as possible. In this context, the functions which may be written as the difference of two convex functions constitute a first set of non convex functions. Some properties associated with the convexity may be used in order to formulate some extremality characterizations [4, 15, 19] and to define appropriate solution algorithms.

In this article we are interested to modelize the buckling of *flexible* and *inextensible* rods. We consider a minimization problem on the displacement field **u** under a non convex equality constraint. Two algorithms are derived from a special splitting of the Lagrangian into the difference of two convex functions (DC). They are compared to the augmented Lagrangian methods used in this context. These DC formulations are easily extended to contact problems and applied to the determination of confined buckling shapes.

2. A Non Convex Equality Constraint

We consider a thin rod of length ℓ and we assume that the deformed configuration takes place in a 1–2 plane. The configuration is described by a vector function **y** of the curvilinear abscissa s. We restrict ourselves here to the case of an inextensible rod. The inextensibility condition may be written as an equality constraint on the first derivative, with respect to the curvilinear abscissa, of the configuration function,

$$\|\mathbf{y}'(s)\|^2 = \left(\frac{\mathrm{d}y_1}{\mathrm{d}s}(s)\right)^2 + \left(\frac{\mathrm{d}y_2}{\mathrm{d}s}(s)\right)^2 = 1. \tag{1}$$

This assumption leads to consider only the bending term in the expression of the bulk energy. If the rod is submitted to a volume loading field **f** and to a terminal loading force **F** (cf. Figure 1), the potential energy takes the simplified form,

$$J(\mathbf{y}) = \frac{1}{2}\int_0^\ell E(s)I(s)\|\mathbf{y}''(s)\|^2\mathrm{d}s - \int_0^\ell \mathbf{f}(s)\cdot\mathbf{y}(s)\mathrm{d}s - \mathbf{F}\cdot\mathbf{y}(\ell), \tag{2}$$

where E is the Young modulus and I is the inertial momentum (i.e., EI is the (positive) bending stiffness) which may depend on s. Consequently an equilibrium
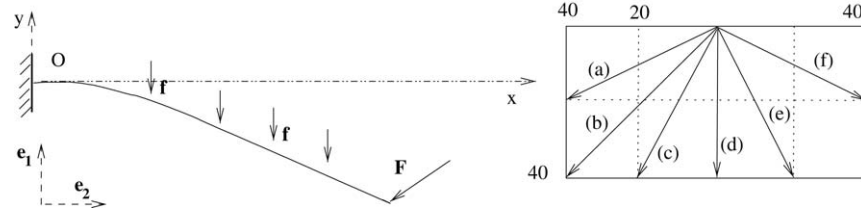
Figure 1. Large bending problem and different loading cases for the force **F**.

state of the rod may be characterized as a local minimum of the potential energy restricted to the kinematically admissible configurations,

$$\inf_{\mathbf{y} \in \mathcal{A} \cap \mathcal{C}} (\mathrm{loc}) J(\mathbf{y}). \tag{3}$$

The set of admissible configurations is the intersection of two sets, the first one containing the boundary conditions, the second one accounting for the inextensibility condition,

$$\mathcal{A} = \{\mathbf{y} \in \mathrm{H}^2(0, \ell); \ \text{plus adequate boundary conditions}\}, \tag{4}$$

$$\mathcal{C} = \{\mathbf{y} \in \mathrm{H}^2(0, \ell); \ h(\mathbf{y}'(x)) = \|\mathbf{y}'(s)\|^2 - 1 = 0 \ a.e. \ s \in]0, \ell[\}. \tag{5}$$

Since the objective function J is convex the non convexity is due to the non convexity of the set $\mathcal{C}$. Indeed the inextensibility condition is expressed with an equality constraint defining a non convex manifold even if the function h in the definition is itself convex.

3. A Convex Difference Mixed Formulation

Using the formulae (2) and (3) we introduce an arbitrary admissible configuration $\mathbf{x}$ in such a way the displacement field $\mathbf{v} = \mathbf{y} - \mathbf{x}$ belongs to the vector sub-space $\mathcal{V}$ associated with $\mathcal{A}$. We define then an affine differential operator D such that $D\mathbf{v} = \mathbf{x}' + \mathbf{v}'$. By this way, the relevant potential energy is expressed as a function of $\mathbf{v}$ and is then denoted φ,

$$\varphi(\mathbf{v}) = \int_0^\ell \left(\frac{EI}{2} \|\mathbf{x}'' + \mathbf{v}''\|^2 - \mathbf{f} . \mathbf{v} \right) \mathrm{d}s. \tag{6}$$

For simplicity the concentrated force at the end is omitted. The local minimization problem is then formulated as a constrained problem on the $\mathbf{v}$ field,

$$\inf_{\mathbf{y} \in \mathcal{A} \cap \mathcal{C}} (\mathrm{loc}) J(\mathbf{y}) \Longleftrightarrow \inf_{\mathbf{v} \in \mathcal{V}, \ h(D\mathbf{v})=0} (\mathrm{loc}) \ \varphi(\mathbf{v}). \tag{7}$$

Starting from (7) we introduce a scalar multiplier field in order to postulate a saddle-point problem for which the Lagrangian function is non convex with respect to the first variable $\mathbf{v}$ and linear with respect to the Lagrange multiplier μ,

$$\inf_{\mathbf{v}\in\mathcal{V}}(\text{loc})\sup_{\mu\in L^2(0,\ell)} L(\mathbf{v};\mu), \tag{8}$$

where $L(\mathbf{v};\mu)=\varphi(\mathbf{v})+\int_0^\ell \mu(s)h(D\mathbf{v}(s))\mathrm{d}s$.
Consequently, it is convenient to write the Euler-Lagrange equations characterizing a *stationary point* $(\mathbf{u},\lambda)$ of the Lagrangian functional,

$$0=\frac{\partial L}{\partial \mathbf{v}}(\mathbf{u};\lambda), \tag{9}$$

$$0=\frac{\partial L}{\partial \mu}(\mathbf{u};\lambda). \tag{10}$$

To deal with the first Equation (9) we introduce the following splitting of the Lagrangian into the *difference of two convex functions*,

$$L(\mathbf{v};\mu)=\Phi_1(\mathbf{v};\mu)-\Phi_2(\mathbf{v};\mu), \tag{11}$$

where,

$$\Phi_1(\mathbf{v};\mu)=\varphi(\mathbf{v})+\int_0^\ell \mu^+(s)h(D\mathbf{v}(s))\mathrm{d}s, \tag{12}$$

$$\Phi_2(D\mathbf{v};\mu)=\int_0^\ell \phi_2(D\mathbf{v};\mu)\mathrm{d}s=\int_0^\ell \mu^-(s)h(D\mathbf{v}(s))\mathrm{d}s. \tag{13}$$

The functions μ^- and μ^+ are defined by,

$$\mu^+(s)=\max(0,\mu(s))\quad\text{and}\quad \mu^-(s)=\max(0,-\mu(s)).$$

The decomposition (12) and (13) uses at best the convexity of h, but a similar approach may be carried out when we have a DC splitting of $h=h_1-h_2$,

$$\Phi_1(\mathbf{v};\mu)=\varphi(\mathbf{v})+\int_0^\ell (\mu^+(s)h_1(D\mathbf{v}(s))+\mu^-(s)h_2(D\mathbf{v}(s)))\mathrm{d}s, \tag{14}$$

$$\Phi_2(D\mathbf{v};\mu)=\int_0^\ell (\mu^-(s)h_1(D\mathbf{v}(s))+\mu^+(s)h_2(D\mathbf{v}(s)))\mathrm{d}s. \tag{15}$$

A *critical point* $\mathbf{u}$ of the potential energy L is defined by,

$$0\in\partial_\mathbf{u}\Phi_1(\mathbf{u};\mu)-\partial_\mathbf{u}(\Phi_2\circ D)(\mathbf{u};\mu). \tag{16}$$

where $\partial_\mathbf{u}$ denotes the subdifferential of a convex function with respect to the variable $\mathbf{u}$. In this expression, for simplicity reason, μ is only considered as a

parameter. Since Φ_1 is a strictly differentiable function [8] the set equality in Equation (16) holds and the previous inclusion is equivalent to,

$$\partial_{\mathbf{u}}(\Phi_2 \circ D)(\mathbf{u}; \mu) \cap \partial_{\mathbf{u}}\Phi_1(\mathbf{u}; \mu) \neq \emptyset. \tag{17}$$

Among the critical points, a *local minimum* $\mathbf{u}$ satisfies[1],

$$\partial_{\mathbf{u}}(\Phi_2(\mathbf{u}; \mu) \subset \partial_{\mathbf{u}}\Phi_1(\mathbf{u}; \mu). \tag{18}$$

Consequently we define a type II Lagrangian depending on three fields by using the Fenchel transform[2] of the second function with respect the first variable,

$$\begin{aligned}
L(\mathbf{v}; \mu) &= \Phi_1(\mathbf{v}; \mu) - \Phi_2(\mathbf{v}; \mu), \\
&= \Phi_1(\mathbf{v}; \mu) - \sup_{\tau}\{D\mathbf{v} : \tau - \Phi_2^*(\tau; \mu)\} \\
&= \inf_{\tau}\left\{\Phi_1(\mathbf{v}; \mu) + \Phi_2^*(\tau; \mu) - \int_{\Omega} D\mathbf{v} : \tau \, \mathrm{d}s\right\} \\
&= \inf_{\tau} L_{\mathrm{II}}(\mathbf{v}, \tau; \mu).
\end{aligned}$$

so we have,

$$L_{\mathrm{II}}(\mathbf{v}, \tau; \mu) = \Phi_1(\mathbf{v}; \mu) + \Phi_2^*(\tau; \mu) - \int_0^{\ell} D\mathbf{v} \cdot \tau \, \mathrm{d}s. \tag{19}$$

This Lagrangian is separately convex in each of the dual variables but not with respect to the couple. A 'saddle point' type problem may be associated to the first Lagrangian L,
   Find $(\mathbf{u}, \sigma, \lambda) \in \mathcal{V} \times \mathrm{L}^2(0, \ell) \times \mathrm{L}^2(0, \ell)$ such that

$$\begin{aligned}
&L_{\mathrm{II}}(\mathbf{u}, \sigma; \mu) \leqslant L_{\mathrm{II}}(\mathbf{u}, \sigma; \lambda) \leqslant L_{\mathrm{II}}(\mathbf{v}, \tau; \lambda), \\
&\forall (\mathbf{v}, \tau; \mu) \in \mathcal{V} \times L^2(0, \ell) \times L^2(0, \ell).
\end{aligned} \tag{20}$$

This treatment of the inextensibility condition leads to a three fields problem (or five scalar fields). Naturally, we can derive from this formulation different solution methods based on the Uzawa algorithm to solve the Equations (9), (10). The first choice consists in solving fully the Equation (9) by a DC algorithm before updating the Lagrange multiplier according to the Uzawa iteration (10), defining the DCalg1 method,

---

[1]This relation fully characterizes a local minimum only if Φ_2 is a piecewise affine function [15]. This property is not true in general for the continuous problem but can be verified in finite dimensional cases, i.e., after finite element approximation.

[2]The density $\phi_2^*(\tau; \mu) = \sup_{D\mathbf{v}}\{D\mathbf{v} : \tau - \phi_2(D\mathbf{v}; \mu)\}$ is the classical Fenchel conjugate function.

DCalg1

- Initialization of the algorithm with $(\mathbf{u}^0, \sigma^0; \lambda^0)$,
- $(\mathbf{u}^{n-1}, \sigma^{n-1}; \lambda^{n-1})$ known, determine $\mathbf{u}^n, \sigma_2^n, \lambda^n$ as follows,

  Step 1: Determination of $(\mathbf{u}^n, \sigma^n)$ by the DC algorithm on $L_{\mathrm{II}}(.,.;\lambda^{n-1})$
         a: $\mathbf{u}^{n,i} = \arg\min L_{\mathrm{II}}(.,\sigma^{n,i-1};\lambda^{n-1})$
         b: $\sigma^{n,i} \in \arg\min L_{\mathrm{II}}(\mathbf{u}^{n,i},.;\lambda^{n-1})$
  Step 2: Updating of the multiplier: $\lambda^n = \lambda^{n-1} + \rho h(D\mathbf{u}^n)$

We recall that the DC algorithm, as introduced by Auchmuty ([4]), consists in minimizing successively the type II Lagrangian L_{II} with respect to the two first variables $\mathbf{v}$ and τ as precised in the two sub steps a and b of the step 1. The second strategy refers to a block relaxation procedure by limiting the DC algorithm to a single iteration leading to the DCalg2 algorithm,

DCalg2

- Initialization of the algorithm with $(\mathbf{u}^0, \sigma^0; \lambda^0)$,
- $(\mathbf{u}^{n-1}, \sigma^{n-1}; \lambda^{n-1})$ known, determine $\mathbf{u}^n, \sigma_2^n, \lambda^n$ as follows,

  Step 1: $L_{\mathrm{II}}(\mathbf{u}^n, \sigma^{n-1}; \lambda^{n-1}) \leqslant L_{\mathrm{II}}(\mathbf{v}, \sigma^{n-1}; \lambda^{n-1}) \; \forall \mathbf{v} \in \mathcal{V}$
  Step 2: $L_{\mathrm{II}}(\mathbf{u}^n, \sigma^n; \lambda^{n-1}) \leqslant L_{\mathrm{II}}(\mathbf{u}^n, \tau, \lambda^{n-1}) \; \forall \tau \in L^2$
  Step 3: $\lambda^n = \lambda^{n-1} + \rho h(D\mathbf{u}^n)$

The first step of the DCalg2 consists then in finding $\mathbf{u}^n$ in $\mathcal{V}$ such that,

$$\int_0^\ell \{EI(\mathbf{x}'' + \mathbf{u}''^n)\cdot\mathbf{v}'' + 2(\lambda^+)^{n-1}(\mathbf{x}' + \mathbf{u}'^n)\cdot\mathbf{v}'\}\mathrm{d}s$$

$$= \int_0^\ell (\mathbf{f}\cdot\mathbf{v} + \sigma^{n-1}\cdot\mathbf{v}')\mathrm{d}s, \quad \forall \mathbf{v}\in\mathcal{V}. \tag{21}$$

For convenience, we summarize the previous formula as follows,

$$(\mathbf{A}^{n-1}\mathbf{u}^n, \mathbf{v}) = (\mathbf{b}^{n-1}, \mathbf{v}) \quad \forall \mathbf{v}\in\mathcal{V}, \tag{22}$$

where $\mathbf{A}^{n-1}$ is a differential operator updated at each DCalg2 iteration.

4. Comparison with the Augmented Lagrangian Approach

At this stage it is interesting to compare this approach to the augmented Lagrangian techniques developed by Glowinsky and Le Tallec [11], specially in the context of flexible and inextensible rods. It is convenient to express the problem (3) with a perturbation function G and to add an auxiliary field $\mathbf{q}$ such that,

$$\inf_{\mathbf{y}\in\mathcal{A}\cap\mathcal{C}}(\mathrm{loc})J(\mathbf{y}) \iff \inf_{\mathbf{v}\in\mathcal{V}}(\mathrm{loc}) \; \varphi(\mathbf{v}) + G(D\mathbf{v}) \tag{23}$$

$$\iff \inf_{(\mathbf{v},\mathbf{q})\in\mathcal{V}\times L^2, \; D\mathbf{v}=\mathbf{q}}(\mathrm{loc}) \; \varphi(\mathbf{v}) + G(\mathbf{q}) \tag{24}$$

where G is the function defined by,

$$G(\mathbf{q}) = \begin{cases} 0 & \text{if } \|\mathbf{q}\| = 1 \ ae \ s, \\ +\infty & \text{otherwise} \end{cases} \tag{25}$$

Lets recall the expression of the augmented Lagrangian for our problem by introducing a *vector multiplier* field to enforce the constraint between the primal variable and the additional field of the problem and a penalty factor r,

$$\mathcal{L}_r(\mathbf{v}, \mathbf{q}; \mu) = \varphi(\mathbf{v}) + G(\mathbf{q}) + \frac{r}{2}\|D\mathbf{v} - \mathbf{q}\|^2 + \int_0^\ell \mu \cdot (D\mathbf{v} - \mathbf{q}) \, ds \tag{26}$$

We associate with this augmented Lagrangian the saddle-point problem,
  Find $(\mathbf{u}, \mathbf{p}, \lambda) \in \mathcal{V} \times L^2 \times L^2$ such that

$$\mathcal{L}_r(\mathbf{u}, \mathbf{p}; \mu) \leqslant \mathcal{L}_r(\mathbf{u}, \mathbf{p}; \lambda) \leqslant \mathcal{L}_r(\mathbf{v}, \mathbf{q}; \lambda), \quad \forall \mathbf{v} \in \mathcal{V}, \quad \forall \mathbf{q} \in L^2 \quad \forall \mu \in L^2. \tag{27}$$

As a major interest of the augmented Lagrangian formulation (27) it can be solved numerically by an algorithm similar to DCalg2 consisting then of three steps per iteration as follows,

ALalg

- Initialization of the algorithm with $(\mathbf{u}^0, \sigma^0; \lambda^0)$,
- $(\mathbf{u}^{n-1}, \mathbf{p}^{n-1}, \lambda^{n-1})$ known, determine $\mathbf{u}^n, \mathbf{p}^n, \lambda^n$ as follows,

  Step 1: $\mathcal{L}_r(\mathbf{u}^n, \mathbf{p}^{n-1}; \lambda^{n-1}) \leqslant \mathcal{L}_r(\mathbf{v}, \mathbf{p}^{n-1}; \lambda^{n-1}) \ \forall \mathbf{v} \in \mathcal{V}$
  Step 2: $\mathcal{L}_r(\mathbf{u}^n, \mathbf{p}^n; \lambda^{n-1}) \leqslant \mathcal{L}_r(\mathbf{u}^n, \mathbf{q}, \lambda^{n-1}) \ \forall \mathbf{q} \in L^2, \|\mathbf{q}\| = 1$
  Step 3: $\lambda^n = \lambda^{n-1} + \rho(D\mathbf{u}^n - \mathbf{p}^n)$

The two approaches need three fields, but the third one is a scalar in the DC formulation and a vector in the augmented Lagrangian method. The two algorithms have three steps with identical characteristics: the first one is a global minimization problem solution, the second one is a local optimization problem solution, the third one is an updating of a multiplier. The first step consists of a linear problem in both cases but with the same left-hand side for the AL method, and with a different left-hand side modified by the value of λ^+ at each iteration for the DC algorithm (cf. Formula 22). Indeed the solution of the first step of ALalg algorithm can be expressed as follows: Find $\mathbf{u}^n \in \mathcal{V}$ such that,

$$\int_0^\ell \{EI(\mathbf{x}'' + \mathbf{u}''^n) \cdot \mathbf{v}'' + r(\mathbf{x}' + \mathbf{u}'^n) \cdot \mathbf{v}'\} ds$$

$$= \int_0^\ell \{\mathbf{f} \cdot \mathbf{v} + (r\mathbf{p}^{n-1} - \lambda^{n-1}) \cdot \mathbf{v}'\} ds, \quad \forall \mathbf{v} \in \mathcal{V}. \tag{28}$$

Formally we can summarize the previous formula as follows,

$$(\mathbf{A}_r \mathbf{u}^n, \mathbf{v}) = (\mathbf{b}_r^{n-1}, \mathbf{v}), \quad \forall \mathbf{v} \in \mathcal{V}, \tag{29}$$

where the differential operator $\mathbf{A}_r$ does not depend on the iteration number. Consequently the linear system solution is cheaper with AL than with DC, specially if a factorization is performed. But the AL algorithm needs two extra parameters, r and ρ since only ρ has to be chosen with DC. The local problem may be solved analytically in both cases as presented below, even if this local problem is not convex for the AL algorithm contrary to DC one of course. The initial minimization problem (3) has to be understood in a local sense, but it seems to us that the ability to reach a local minimum is theoretically better with the DC algorithm where the convexity property is used at best leading to characterizations, as Equation (18), and numerical schemes. Indeed in all the numerical simulations, we get a local minimum of J on $\mathcal{A} \cap \mathcal{C}$ and never a local maximum nor an other critical point.

5. Numerical Implementation and First Applications

It is classical to adopt a finite-element approximation of the Hermite cube type of the displacement field with two degrees of freedom per node: the displacement and its gradient with respect to the curvilinear abscissa. The interval $[0, \ell]$ is decomposed into N_e sub-intervals,

$$0 = s_0 < s_1 < \cdots < s_{i-1} < s_i < s_{i+1} < \cdots < s_{N_e} = \ell.$$

According to the approximation of the displacement by piecewise polynomials of degree less than or equal to three – the associated space is noted P^{3-}, we need to define the discrete variables of $\mathbf{p}$ and λ at the three Gauss-Legendre points noted $s_{i+\alpha}, s_{i+1/2}, s_{i+1-\alpha}$ of each finite element $[s_i, s_{i+1}]$. Then the second step of the two algorithms is performed at the Gauss-Legendre points and is very simple. For ALalg the second minimization problem becomes,

$$\begin{cases} \forall s \in S = \bigcup_{i=0}^{N_e-1} \{s_{i+\alpha}, s_{i+1/2}, s_{i+1-\alpha}\}, \quad \text{find } \mathbf{p}^n(s) \in \mathbb{R}^3 \text{ such that } \|\mathbf{p}^n(s)\| = 1, \\ \text{and} \\ \dfrac{r}{2} \|D\mathbf{u}^n(s) - \mathbf{p}^n(s)\|^2 - \lambda^{n-1}(s) \cdot \mathbf{p}^n(s) \leqslant \dfrac{r}{2} \|D\mathbf{u}^n(s) - \mathbf{q}\|^2 - \lambda^{n-1}(s) \cdot \mathbf{q}, \\ \forall \mathbf{q} \in \mathbb{R}^3 \quad \text{with } \|\mathbf{q}\| = 1, \end{cases}$$

and its solution is given by,

$$\mathbf{p}^n(s) = (\tau D\mathbf{u}^n(s) + \lambda^{n-1}(s)) / \|\tau D\mathbf{u}^n(s) + \lambda^{n-1}(s)\|, \quad \forall s \in S. \tag{30}$$

Table 1. Criteria for the AL and DC algorithms

Criteria for the AL algorithm	Criteria for the DC algorithms
$$\frac{\int_0^\ell \|\mathbf{u}^n - \mathbf{u}^{n-1}\|^2 + \|D\mathbf{u}^n - D\mathbf{u}^{n-1}\|^2 \, ds}{\int_0^\ell \|\mathbf{u}^n\|^2 + \|D\mathbf{u}^n\|^2 \, ds} \leqslant \varepsilon_1$$	idem
$$\frac{1}{\sqrt{\ell}} \int_0^\ell \|D\mathbf{u}^n - \mathbf{p}^n\|^2 \, ds \leqslant \varepsilon_2$$	$$\frac{1}{\sqrt{\ell}} \int_0^\ell h(D\mathbf{u}^n) \, ds \leqslant \varepsilon_2$$

For DC algorithms the solution is given by,

$$\sigma^n(s) = \nabla_{V'}\phi_2(\mathbf{u}'^n; \lambda^{n-1}) = 2(\lambda^-)^{n-1} D\mathbf{u}^n(s), \quad \forall s \in S. \tag{31}$$

In order to compare AL and DC algorithms, we chose the following stopping criteria, cf. Table 1. The computation is stopped when the two criteria are satisfied.

The first criterion coincides in both cases, but the second one is different because the equality constraint is not the same: the DC algorithm verifies the inextensibility condition directly since the AL algorithm controls the gap between the gradient of the configuration field and the additional field $\mathbf{p}$.

To compare the performance of the different algorithms we study the problem of the large bending of a rod, of length ℓ, clamped at the origin and submitted to a terminal loading force $\mathbf{F}$ with different directions as represented in the Figure 1b; the deformed shapes are plotted in the Figure 2b. The data are: $\ell = 10\text{m}$, $EI = 1000\text{N/m}^2$. Six finite elements are performed; the convergence thresholds are $\varepsilon_1 = 10^{-7}$ and $\varepsilon_2 = 10^{-3}$; the parameters $\rho = 20$ for DC algorithms, $\rho = 20$ or 200 and $r = 20$ or 200 for ALalg. The Table 2 gives the behaviour of the three algorithms, DCalg1, DCalg2, ALalg in terms of number of iterations; for DCalg1 the number of internal iterations of the DC algorithm is specified between brackets. The DC algorithms converge generally faster than the AL method with the same factor ρ. It is usual to chose in Augmented Lagrangian method ρ equal to r. This choice leads to better results for cases (e) and (f) for which the non convexity is weakly active (see comments below), but the ALalg does not converge for the cases characterized by a strong non convexity; DCalg1
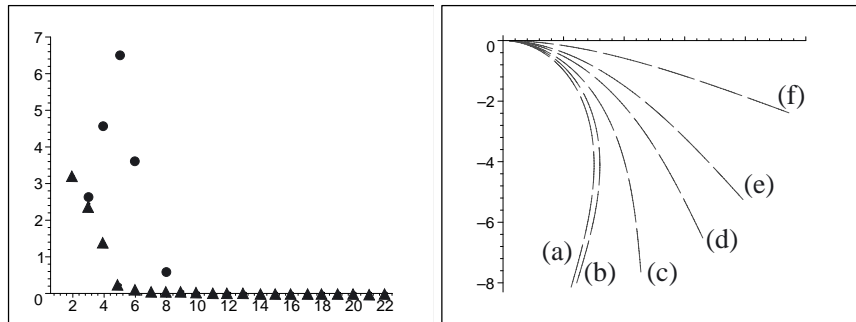

Figure 2. Characteristic criteria evolution and the deformed shapes (six elements).

Table 2. Behaviour of the three algorithms (6 elements, 3×6 Gauss points)

Loading force	(a)	(b)	(c)	(d)	(e)	(f)
Nb of iterations DCalg1 (internal loops)	Div	35(7)	30(5)	22(3)	21(2)	29(1)
Nb of iterations DCalg2	37	33	28	22	21	29
Nb of iterations ALalg ($r = 200$, $\rho = 20$)	58	71	45	36	46	55
Nb of iterations ALalg ($r = \rho = 200$)	∞	∞	24	22	18	16
Nb of iterations ALalg ($r = \rho = 20$)	∞	∞	∞	∞	15	38
Nb of Gauss points: $\lambda = \lambda^-$	11	8	8	5	2	0
Nb of Gauss points: $\lambda = \lambda^+$	7	10	10	13	16	18

may not converge in the case (a). The internal loop of DCAlg1 does not improve the global convergence of the algorithm, but this conclusion concerns only this numerical test which is simpler than the buckling test of the following section. The influence of the non convexity is well underlined: the number of internal iterations increases as the number of Gauss-Legendre points where λ is negative, which is related to the non convexity. We observe that the internal iterations are reduced to a single for the case (f) which corresponds to a locally convex problem (any Gauss point with λ^- non null). The Figure 2a shows the evolution of the two criteria according to the iterations (DCalg2) for one loading case. The second criterion, marked ▲, on the inextensibility condition decreases quickly and monotonically since the first, marked ●, –which is multiplied by 100 for scaling the two curves-may have a maximum before decreasing.

6. Improvement of the Algorithm for Buckling

Taking into account the inextensibility condition becomes specially crucial as soon as large displacements occur. Such a situation concerns for instance flexible pipelines used in offshore oil production [11] and overall the post buckling of rods. In a previous paper [3], we showed that the Elastica theory coupled with a DC algorithm is able to deal with some specific buckling problems induced by a concentrated terminal force. But we cannot handle this approach to treat distributed solicitations and imposed displacements. On the contrary, the previous strategy based on a constrained problem in term of displacement field may deal formally with displacement or force imposed boundary conditions. Nevertheless the two first algorithms (DCalg1 and DCalg2) fail to converge toward a postbuckling shape. Because the problem of the first step is uncoupled in term of the vertical and horizontal components of the displacement, the algorithms tend to reach the trivial solution ($\mathbf{u} = 0$). In other words, the coupling between components is only performed by the inextensibility condition. To overcome this difficulty, we propose to modify the initial minimization problem by adding a quadratic term to the functional φ,

$$\varphi_{\mathbf{W}}(\mathbf{v}) = \varphi(\mathbf{v}) + \int_0^\ell (\mathbf{v} - \mathbf{w}) \cdot \mathbf{A}(\mathbf{v} - \mathbf{w}) \, \mathrm{d}s, \tag{32}$$

and we denote $(P_{\mathbf{W}})$ the minimization problem associated with $\mathbf{w}$. The matrix $\mathbf{A}$ has to be symmetric positive definite and overall non diagonal; in the numerical simulations we choose $\mathbf{A} = a\left(\begin{smallmatrix} 2 & 1 \\ 1 & 2 \end{smallmatrix}\right)$ where a is a strictly positive coefficient. The $\mathbf{w}$ field is a given arbitrary field. Only the first step of the algorithms is modified but stays a linear problem solution; the $\varphi_{\mathbf{W}1}$ function is still strictly convex and coercive in order to assure a well-posed problem. Of course the solutions of the problem $(P_{\mathbf{W}})$ depend on the a factor and the $\mathbf{w}$ field. It is convenient to see a solution of the initial problem as a limit of $(P_{\mathbf{W}})$ type solutions, in such a way the effects of a and $\mathbf{w}$ vanish at the convergence. Consequently we consider the iterative scheme, based on the DCalg1 algorithm, where the first step is performed by replacing the type II Lagrangian L_{II} by the new functional depending on the previous iteration,

$$L_{\mathrm{II}}^{n}(\mathbf{v}, \tau; \mu) = L_{\mathrm{II}}(\mathbf{v}, \tau; \mu) + \int_{0}^{\ell} (\mathbf{v} - \mathbf{u}^{n}) \cdot \mathbf{A}(\mathbf{v} - \mathbf{u}^{n}) \mathrm{d}s. \tag{33}$$

Contrary to the examples presented in the third section, the convergence is not monotonic for the two criteria (cf. Figure 3). We note an opposite evolution of the two criteria during the iterations which characterizes the influence of the additional term. Indeed the coupling between the two components of the displacement due to the additional term enforces to satisfy the first criterion, minimizing the norm between two successive solutions even if these solutions satisfy coarsely the inextensibility condition (second criterion). More precisely we can distinguish an alternative convergence. For instance the iterates 31 and 61 provide upper bounds for the solution shape; the iterates 46 and 76 give lower bounds (cf. Figure 3). All examples presented in Figures 4, 5 and 6 concern a horizontal imposed displacement at the end of the rod with different boundary conditions. If the rod is simply supported, the evolution of the deformed shapes is a continuous process as illustrated in the Figure 4a. By imposing a specific initial shape, we can enforce the algorithm to converge toward others buckling branches (cf. Figure 4b). An interesting result concerns the fourth branch; at first it is obtained from a rustic initialization (cf. Figure 4c) which only satisfies the
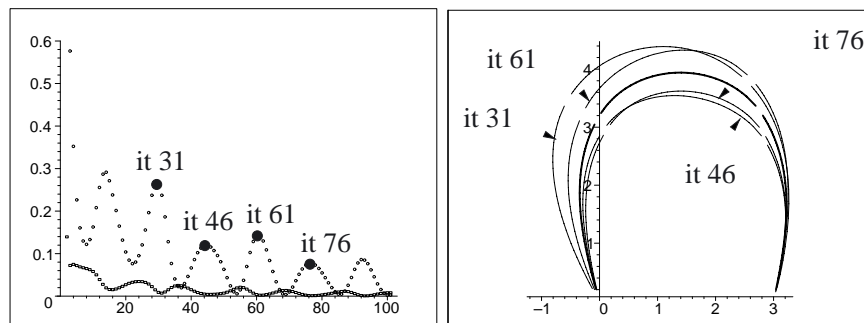

Figure 3. Evolution of the two criteria and shape of some iterates (three elements).
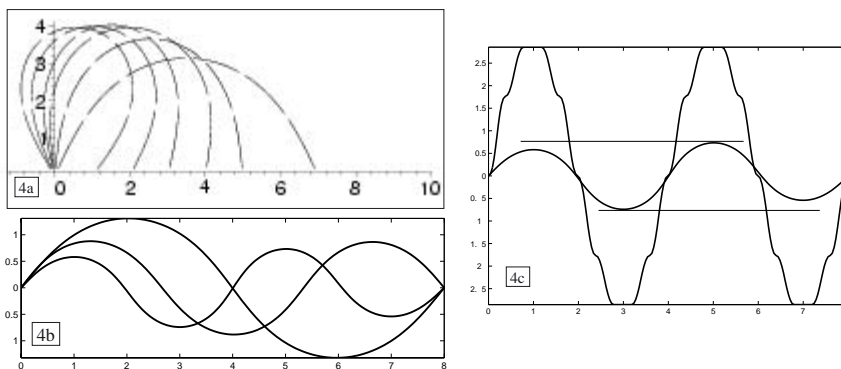
Figure 4. (a) Some shapes for different imposed displacements (6 finite elements). (b) Secondary branches for a same problem (20 finite elements). (c) Initialization of the algorithm and the fourth buckling branch.
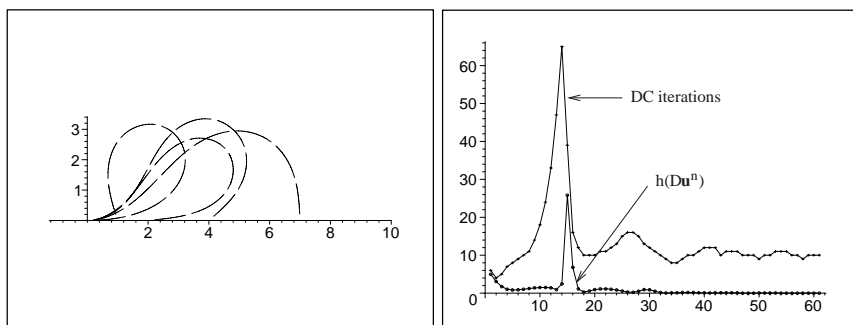

Figure 5. (a) Clamped-just supported (6 finite elements). (b) Number of DC iterations and convergence of the first criterion for the turn case.
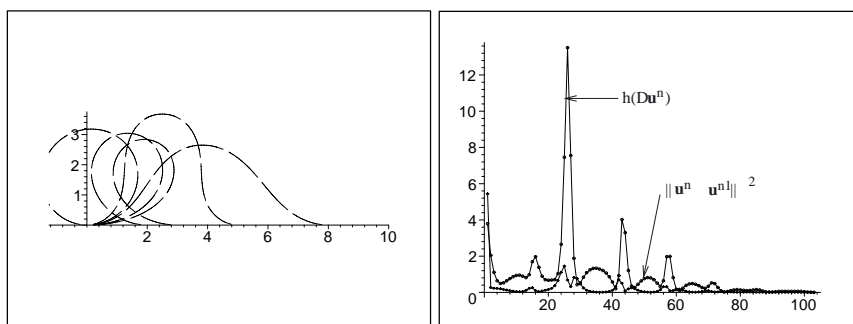

Figure 6. (a) Clamped-clamped (6 finite elements). (b) Convergence of the two criteria for the first turn case.

number of oscillations. Secondly the final shape reveals that the extrema in the middle of the shape are higher than the others (cf. Figure 4c). For the two other cases, with one or two clamped extremities, the evolution may be discontinuous (cf. Figure 5a). If the origin is clamped and for a large imposed displacement, a peak on the second criterion occurs when the shape turns around the fifteenth iteration. Before this iteration the number of DC iterations increases significantly until sixty. After that, this number goes down to ten on average until convergence (cf. Figure 5b). For the fully clamped rod, we have a similar behaviour: the rod buckles to a hat like shape for the 'small' displacements and to piano string like shape for larger values. The first peak occurs when the iterates pass quickly from the hat like shape to the string like shape as shown in Figures 6a and 6b. The secondary peaks correspond to situations previously described in the Figure 3. This behaviour may be related to the jump occurring when an incremental loading is performed but the change of shape needs a three dimensional and dynamical modelling.

7. Unilateral Contact and Confined Buckling

We now consider a flexible rod that can enter in contact with two flat obstacles located below and above the rod at the distances d_a and d_b. If we assume this contact to be frictionless it can then be handled mathematically by introducing two inequalities in the definition of the admissible configurations. The space $\mathcal{A}$ becomes a set defined as follows,

$$\mathcal{A} = \{\mathbf{y} \in H^2(0, \ell); \ -d_a \leqslant y_2 \leqslant d_b \text{ plus adequate boundary conditions}\}, \quad (34)$$

and the sub space $\mathcal{V}$ is replaced by the convex set $\mathcal{K}$,

$$\mathcal{K} = \{\mathbf{v} \in \mathcal{V}; \ -d_a \leqslant (x_2 + v_2)(s) \leqslant d_b \ \ \forall s \in [0, \ell]\}. \quad (35)$$

By denoting N the linear operator such that $N\mathbf{v} = x_2 + v_2$ this convex constraint may be taken into account by a classical constrained optimization problem at the global level of the DC algorithm. Thus the first step of the DCalg2 (or DCalg1) algorithm stays a well-posed problem solution by adding the contact constraint. We have then a constrained quadratic minimization problem. We choose to verify the contact condition at the middle point of the elements in such a way we define the operator $\bar{N}$ from $\mathbb{R}^{4(N_e+1)}$ into $\mathbb{R}^{N_e}$. By denoting $\mathbf{v}$ (resp. $\mathbf{u}$) the generalized nodal displacements associated with a Hermite cube interpolation, the approximated displacement field $\mathbf{v}_h$ can by written as, $\mathbf{v}_h = \mathbf{B}\mathbf{v}$. The approximated admissible set $\mathcal{K}_h$ is now equal to,

$$\mathcal{K}_h = \{\mathbf{v}_h \in \mathcal{V} \cap P^3; \ -d_a \mathbf{1} \leqslant N\mathbf{v}_h(s_{i+1/2}) \leqslant d_b \mathbf{1}, \ \forall i \in \{0, \ldots, N_e\}\}, \quad (36)$$

where $\mathbf{1}$ is the N_e vector for which all components are equal to 1. The discretized admissible set $\mathbb{K}$ can be written as follows,

$$\mathbb{K} = \{\mathbf{v} \in \mathbb{R}^{4(N_e+1)}; -d_a\mathbf{1} \leqslant N(\mathbf{Bv})(s_{i+1/2}) \leqslant d_b\mathbf{1}, \forall i \in \{0,\ldots,N_e\}\} \tag{37}$$

$$= \{\mathbf{v} \in \mathbb{R}^{4(N_e+1)}; -d_a\mathbf{1} \leqslant \bar{\mathrm{N}}\mathbf{v} \leqslant d_b\mathbf{1}\}. \tag{38}$$

where the second formula is a summarized expression.

Let introduce the Lagrange multiplier identified to the contact reaction on the upper or lower side, $\mathbf{R} \in \mathbb{R}^{N_e}$; the same Lagrange multiplier is used for both sides since the contact constraint may be not active simultaneously. We can so define a bi-unilateral contact law [1]. In order to generalize later to frictional contact we use a Generalized Newton method which involves a single loop to solve this non linear problem. At the iteration n, we have to find $(\mathbf{u}^n, \mathbf{R}^n)$ such that,

$$\begin{cases} \mathbf{A}^{n-1}\mathbf{u}^n + \bar{\mathrm{N}}^* \ \mathrm{prox}_{\psi^*_{r[-d_a,d_b]^{N_e}}} (-\mathbf{R}^n + r\bar{\mathrm{N}}\mathbf{u}^n) = \mathbf{b}^{n-1} \\ \dfrac{1}{r}\left\{\mathbf{R}^n + \ \mathrm{prox}_{\psi^*_{r[-d_a,d_b]^{N_e}}} (-\mathbf{R}^n + r\bar{\mathrm{N}}\mathbf{u}^n)\right\} = 0 \end{cases} \tag{39}$$

where $[-d_a, d_b]^{N_e}$ notes a hypercube in $\mathbb{R}^{N_e}$ and $\mathbf{A}^{n-1}$ and $\mathbf{b}^{n-1}$ are now respectively the discrete version of the differential operator and of the right-hand side defined in (22) [2]. The proximal operator is defined in our case as follows [12,18]:$\mathrm{prox}_{\psi^*_C} y = y - \mathrm{proj}_C y$, where ψ^*_C is the support function of the convex set C.

With these numerical modifications, some confined buckling configurations may be determined according to different values of the distance d_a (d_b is always taken equal to d_a). The previous values of ℓ and EI are used again, the coefficient r of the contact operator is taken around the value of EI and the number of elements is fixed to twenty. In the Figure 7 the two extremities of the rods are just supported and the imposed displacement of the end of the rod is fixed to 2m. With d_a equal to 2.7m we have just a grazing contact associated with the first buckling
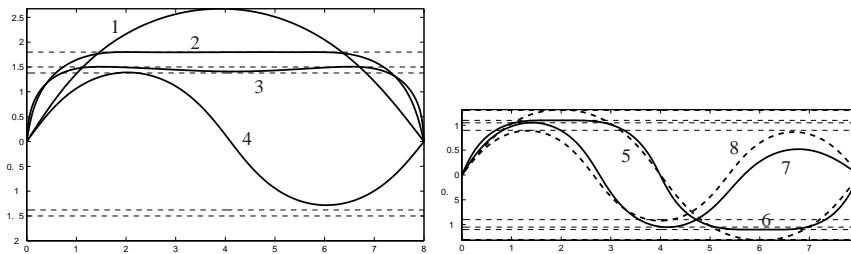

Figure 7. Some confined buckling shapes (20 finite elements): (a) curve 1 ($d_a = 2.7$m, grazing contact), curve 2 ($d_a = 1.8$m, 1 top line contact), curve 3 ($d_a = 1.5$m, 2 top line contacts), curve 4 ($d_a = 1.4$m, 1 top point contact); (b) curve 5 ($d_a = 1.3$m, 2 point contacts, top and bottom), curve 6 ($d_a = 1.1$m, 2 line contacts, top and bottom), curve 7 ($d_a = 1.05$m, 2 point contacts, top and bottom), curve 8 ($d_a = 0.9$m, 3 point contacts, top, bottom and top).

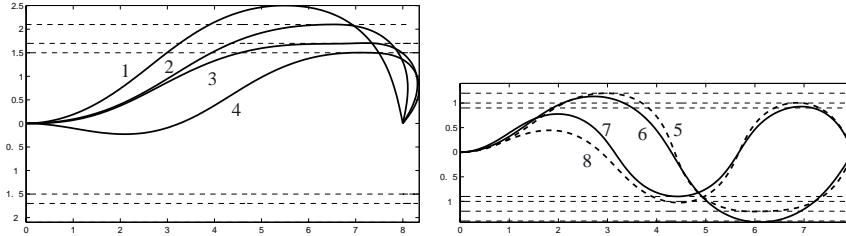*Figure 8.* Some confined buckling shapes (20 finite elements): (a) curve 1 ($d_a = 2.5$m, grazing contact), curve 2 ($d_a = 2.1$m, 1 top line contact), curve 3 ($d_a = 1.7$m, 2 top line contacts), curve 4 ($d_a = 1.5$m, 1 top point contact); (b) curve 5 ($d_a = 1.4$m, 1 bottom point contact), curve 6 ($d_a = 1.2$m, 1 top point contact and 1 bottom line contact), curve 7 ($d_a = 1.0$m, 1 bottom line contact and 1 top point contact), curve 8 ($d_a = 0.9$m, 2 points contacts, top and bottom).

branch. Until 1.8m the contact area increases and reaches 5m around. After that the contact area on the upper side is splitted into two parts (example with d_a equal to 1.5m in the Figure 7a). For 1.4m, the rod jumps to a second branch like configuration with a single top point contact. The second point contact on the lower side occurs since d_a equals 1.3m (cf. Figure 7b). A same process between the first and second branches may be described from the second to the third branch. Specially for d_a equal to 1.05m we recover a third branch like configuration with two point contacts, and the second maximum is far from the upper wall. In the Figure 8 a similar numerical experiment is performed with a clamped origin and a simply supported end. Eight successive shapes are plotted and the different contact conditions are detailed in the captions of the figure. These behaviours have been observed on experiments at least for the first and second branches [7, 9].

8. Numerical Experiments on a Cellular Medium

We study the behaviour of a cellular medium resulting of an assembly of rods. In fact, each unit cell of the network is made with 6 rods connected rigidly (cf. Figure 9): the angle between two rods is assumed to be independent of the deformation (cf. Figure 9b). To deal with this constraint the rod are oriented and
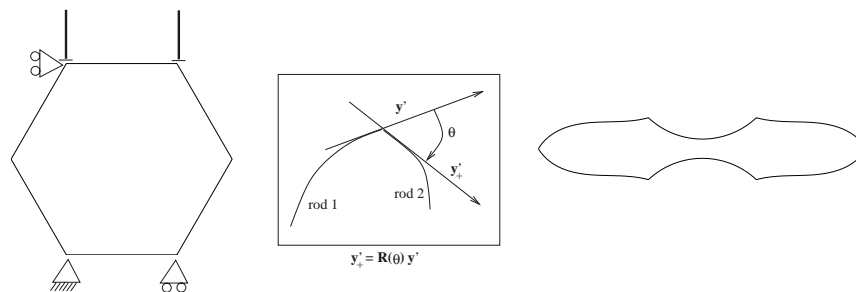

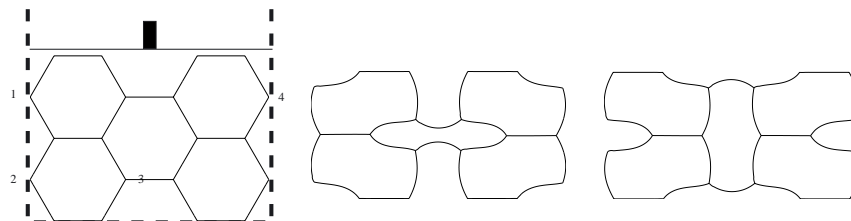*Figure 9.* Boundary conditions and deformed shape for 1 cell.

Figure 10. (a) The horizontal displacement of the points 1, 2, 3 and 4 is null imposed. (b) Two dual patterns for 5 cells.
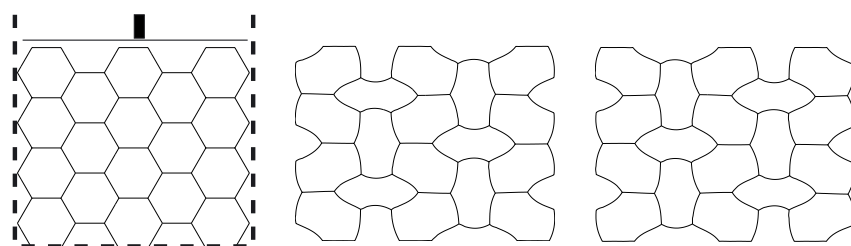

Figure 11. Boundary conditions and buckled shapes for 18 cells.

at a junction point the right-derivative of the second rod is connected to left-derivative of the first one by a rotation $R(\theta)$. Recall that in non linear elasticity the homogenization procedure cannot provide an effective behaviour law for the honeycomb material starting from one unit cell as the elementary representative volume [13]. However to investigate the behaviour of such a structure in some situations we consider an increasing number of cells in a specimen. We hope then to capture the possible configurations paths, at least until the self contact. The studied case is a confined compression test consisting of a specimen pressed into a box on its upper side. For convenience the boundary conditions are approximated without taking into account unilateral contact conditions between the structure and the box. Only 6 elements are used for each rod. The buckled configuration is recovered numerically (cf. Figure 9c). With 5 cells we get two dual patterns according to the initialization of the algorithm (cf. Figure 10). With 18 cells (4 times the previous sample), two buckled configurations combine by two ways the patterns observed with 5 cells (cf. Figure 11). Although these examples are geometrically more complex than the buckling of a single rod, presented in a previous section, the algorithm needs a regularization parameter *a* smaller leading to a faster convergence.

9. Conclusion

After previous works [16, 19], the study developed in this paper confirms the ability of the convex difference formulation to determine local minima of some non convex potentials in non linear mechanics. The present approach allows also to

deal with a non convex equality constraint. Our method uses a standard Lagrange multiplier before splitting the potential. Pham Dinh and Hoai An obtain a DC decomposition directly by reformulating the problem [17]; but their procedure introduces also an extra parameter. The algorithms DCalg1 and DCalg2 are more efficient than the augmented Lagrangian method [11] because they use at best the convex properties of the problem. But the buckling phenomena proves difficult to simulate because the coupling between the axial and transverse components is only assured by the inextensibility condition. Consequently a vanishing term has to be added to the objective function to minimize. The introduction of contact conditions preserves the DC structure of the problem and of the algorithms; the first step is just enriched with a contact convex constraint. The contact zones are not known a priori and we can note that among our results some equilibrium states may not be determined analytically. The method may deal with reticular structures or cellular materials composed of many rods and provides some complex buckled branches.

The following step of this study would consist of the tridimensional modelling of rods with confinement in a tube with application to pushing of long cables. Moreover the behaviour of cellular structure needs to account for the self contact in the closure of the cells. This phenomena is essential in the densification process of the wood for instance.

Finally the previous approach may be easily extended to the buckling of plates and shells for which the inextensibility condition is expressed with two relations similar to (1) [6].

References

1. Ach, K. and Alart, P. (2001), Numerical simulation of the behaviour of a multi-jointed structure, *Phil. Trans. R. Soc. Lond. A*, 359, 2557–2573.
2. Alart, P. and Curnier, A. (1991), A mixed formulation for frictional contact problems prone to newton like solution methods, *Comp. Meth. Appl. Mech. Eng.*, 92, 353–375.
3. Alart, P. and Pagano, P. (2001), Convex difference algorithm and applications to some mechanical problems, in press.
4. Auchmuty, G. (1989), Duality algorithms for nonconvex variational principles, *Num. Funct. An. and Opt.*, 10, 211–264.
5. Bloom, F. and Coffin, D. (2001), *Handbook of Thin Plate Buckling and Postbuckling*, Chapman and Hall, Boca Raton, Florida.
6. Casarino, V. and Percivale, D. (1996), A variational model for non linear elastic plates, *J. Convex Anal.*, 3(2), 221–243.
7. Chateau, X. and Nguyen, Q.S. (1991), Buckling of elastic structures in unilateral contact with or without friction, *Eur. J. Mech A*, 10, 71–89.
8. Clarke, F.H. (1993), *Optimization and Nonsmooth Analysis*, A Wile-interscience publication, New York.
9. Domokos, G., Holmes, P. and Royce, B. (1997), Constrained Euler buckling, *J. Nonlinear Sci.*, 7, 281–314.
10. Euler, L. (1744), Additamentum i de curvis elastics, methodus inveniendi lineas maximi minimiui proprietate gaudentes, *Bousquent, Lausanne; in Opera Omnia*, 24, 231–297.

11. Glowinski, R. and Le Tallec, P. (1989), *Augmented Lagrangian and Operator-Splitting Methods in Nonlinear Mechanics*, SIAM Studies in Applied Mathematics, Philadelphia, PA.

12. Moreau, J.J. (1967), Fonctionnelles convexes. In: *Séminaire sur les Equations aux Dérivées particlles*, Collège de France, Paris.

13. Müller, S. (1987), Homogenization of non convex integral functionals and cellular elastic materials, *Arch. Ration. Mech. Anal.*, 99, 189–212.

14. Nguyen, Q.S. (2000), *Stabilité et mécanique non linéaire*, Hermés Science Publications, Paris.

15. Pagano, S. (1997), (*Quelques aspects de*) *la modélisation numérique du comportement des alliages à memoire de forme par des potentiels non convexes*. PhD thesis, Univ. Montpellier II, France.

16. Pagano, S., Alart, P. and Maisonneuve, O. (1998), Solid-solid phase transition modelling. local and global minimizations of nonconvex and relaxed potentials. isothermal case for shape memory alloys, *Int. J. of Eng. Sci.*, 36, 1143–1172.

17. Pham Dinh, T. and Hoai An, L.T. (1998), A d.c. optimization algorithm for solving the trust-region subproblem, *SIAM J. Optim.*, 8(2), 476–505.

18. Rockafellar, R.T. (1970), *Convex Analysis*, Princeton U.P.

19. Stavroulakis, G.E. and Panagiotopoulos, P.D. (1993), Convex multilevel decomposition algorithms for non-monotone problems, *Int. Journ. for Num. Meth. in Eng.*, 36, 1945–1966.